Table S1. List of MCMv3.2 species used to model the ester oligomer formation in Section 3.3.3.

C722OOH

C920CO3H

HOPINONIC

C516OOH

C920PAN

C811PAN

PINIC

NC101OOH

C108OH

C813OH

C922OOH

C811OH

C813OOH

C98OOH

C811OOH

C89CO2H

C621OOH

C812OH

PINONIC

C98OH

C811CO3H

C920OOH

C812OOH

C813NO3

C97OOH

NORPINIC

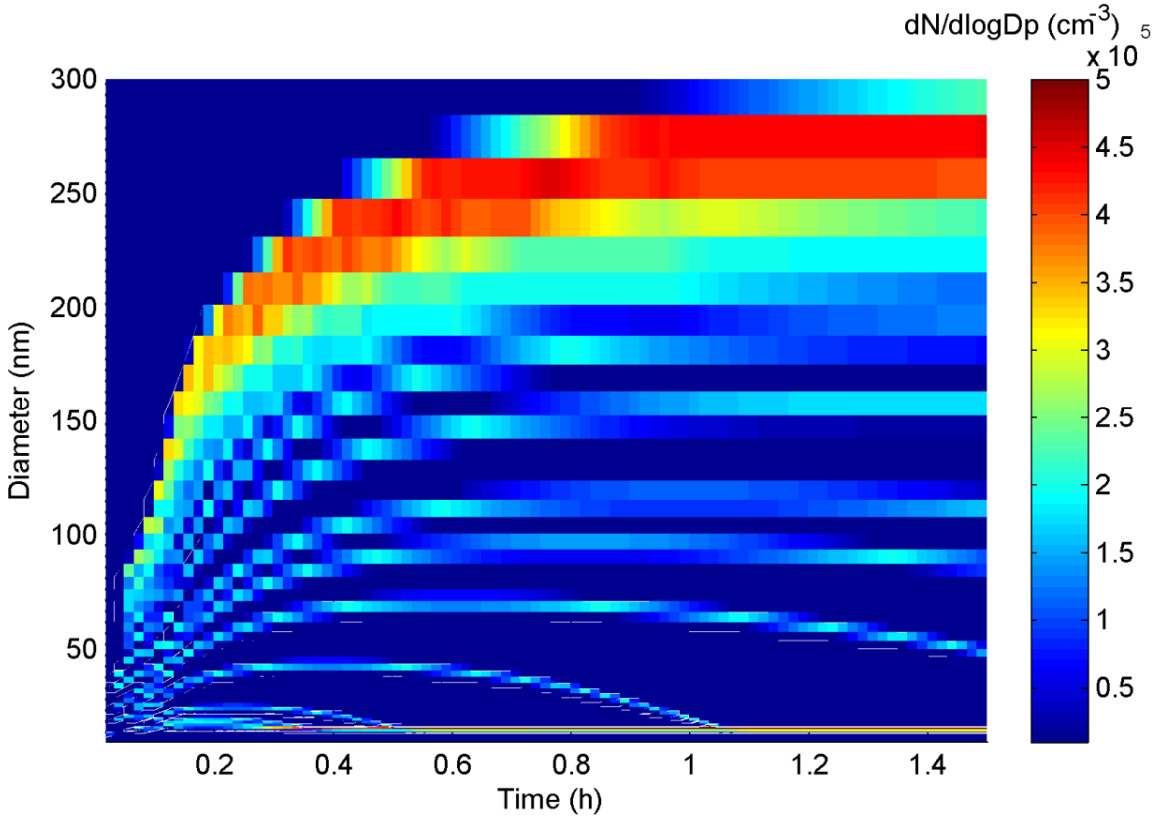

Figure S1. Modelled temporal evolution of the particle number size distribution. The results presented in this figure are from a simulation with initially 200 ppb α-pinene, 500 ppb O_3 and 250 ppm cyclohexane as OH-scavenger, semi-solid particles, no oligomerization and with pure-liquid saturation vapour pressures from the SIMPOL method. The condensational growth of the particles was modelled with the full moving method (Sect. 2.2.4). However, the particle number size distribution was converted to a fixed diameter grid for the plot.

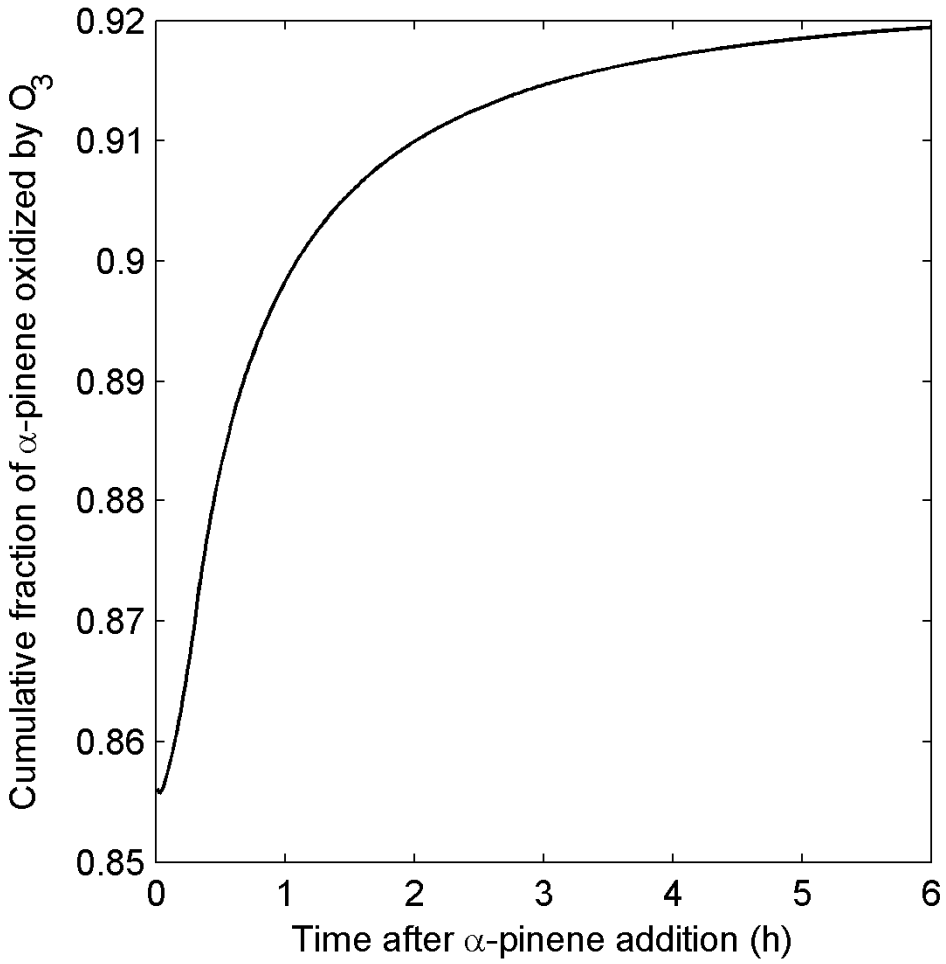

Figure S2. Cumulative fraction of α-pinene oxidized by O_3 for the modelled experiments from Na et al. (2007).

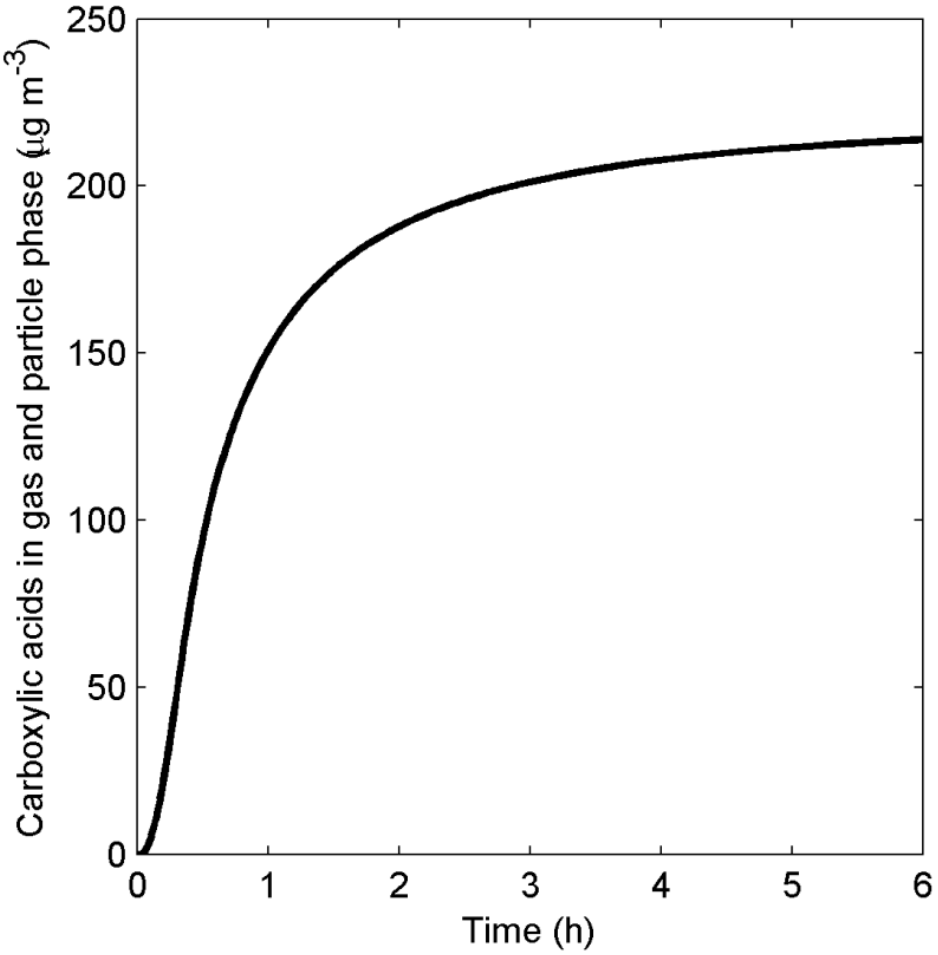

Figure S3. Modelled total carboxylic acids concentration in the gas and particle phase during the α-pinene oxidation experiments from Na et al. (2007).

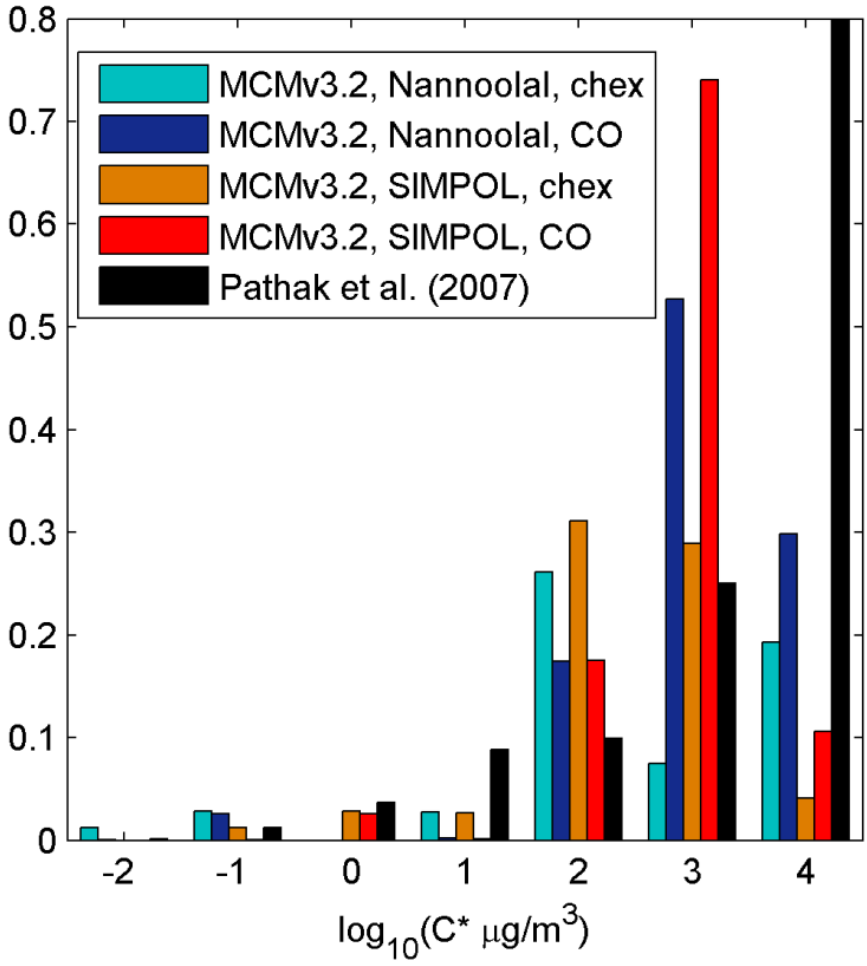

Figure S4. Derived VBS from the simulated α-pinene oxidation experiments from Na et al. (2007) with CO as OH scavenger, and from Vaden et al. (2011) with cyclohexane as OH scavenger. The VBS parameterizations were derived with the pure-liquid saturation vapour pressure method from Nannoolal et al. (2008) and SIMPOL (Pankow and Asher, 2008). Given is also the experimentally derived VBS parameterization from Pathak et al. (2007).

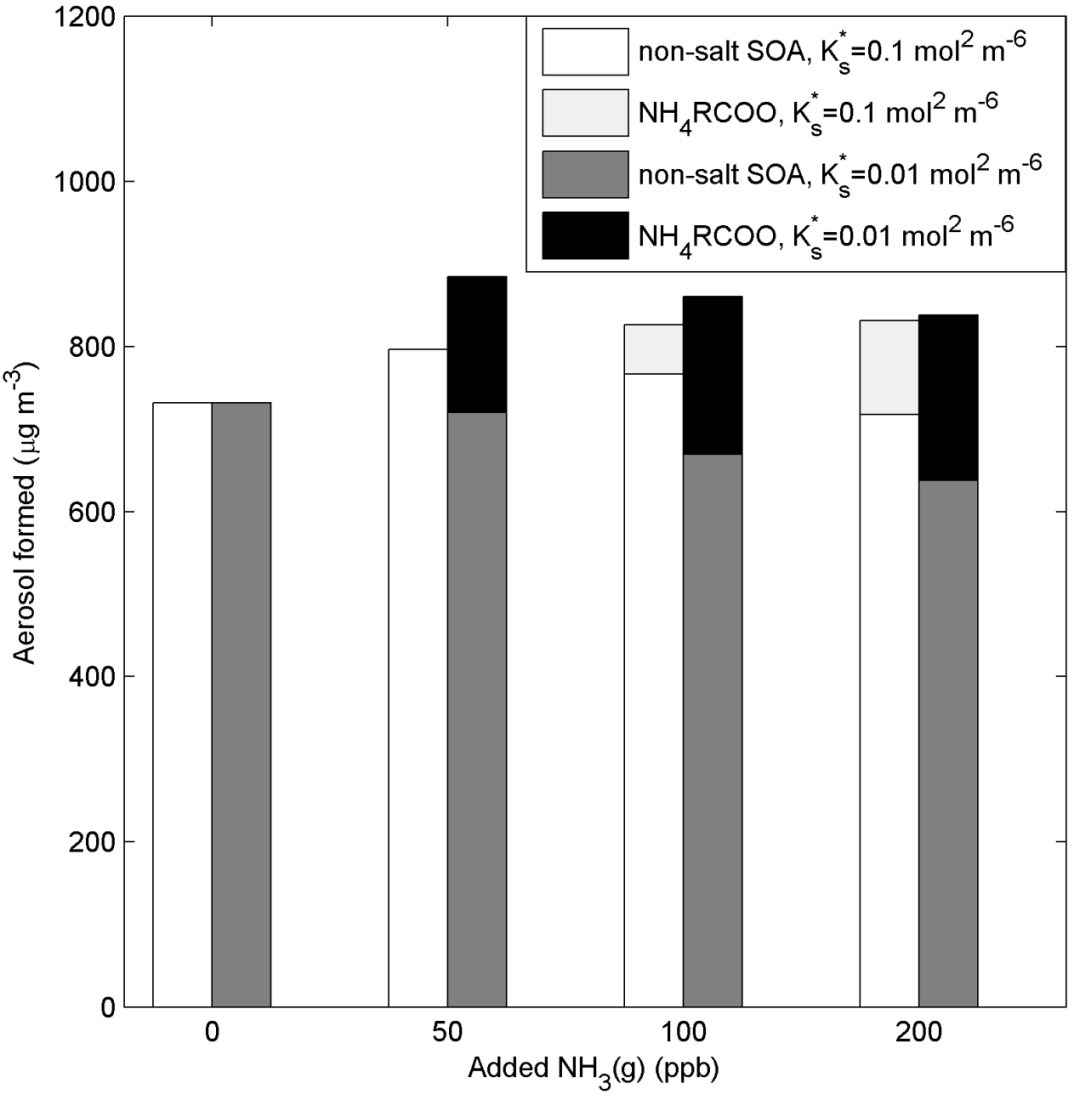

Figure S5. Comparison of modelled SOA mass formation with an effective solubility product (K_s^*) of 0.01 or 0.1 mol^2 m^{-6} (Eq. 32) for the organic salts of carboxylic acids and ammonium (NH_4RCOO). The total aerosol mass is divided into the fraction composed of non-salt SOA and NH_4RCOO.

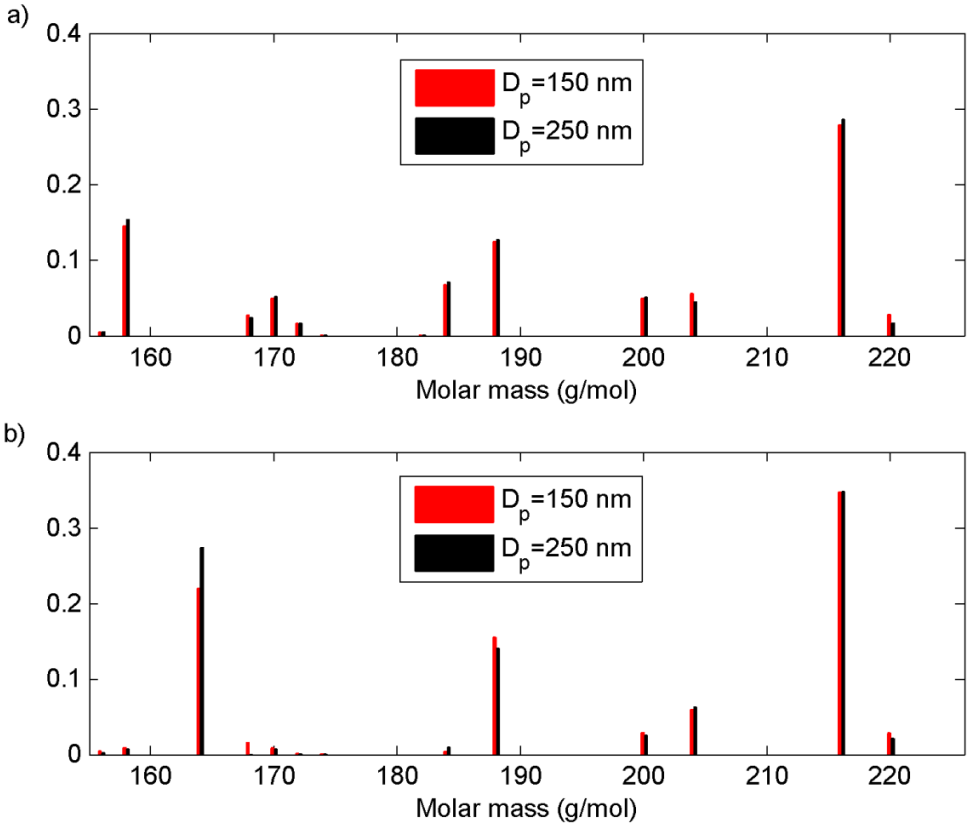

Figure S6. Modelled monomer mass spectrum of solid SOA particles formed by ozonolysis of α-pinene. (a) with the SIMPOL saturation vapour pressure method and (b) with the saturation vapour pressure method from Nannoolal et al. (2008). The low volatile MCMv3.2 oxidation product C922OOH has a mass peak at 220 g/mol.

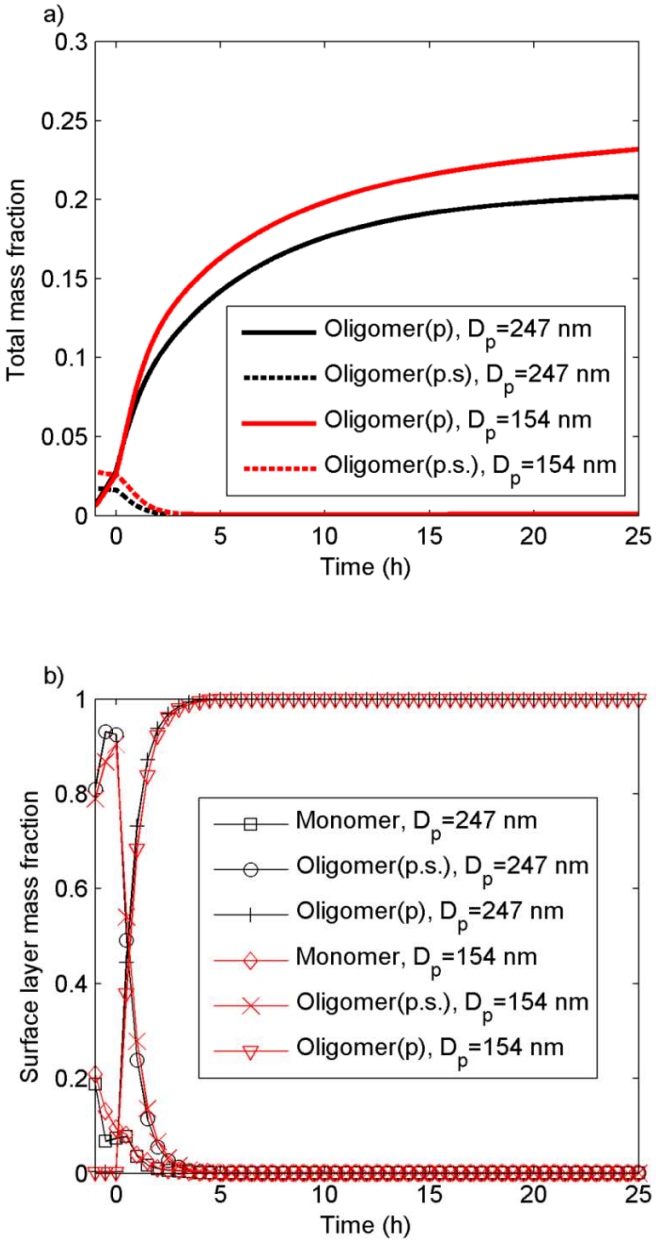

Figure S7. Modelled total single particle oligomer mass fraction (a), and monomer, surface oligomer and bulk oligomer mass fraction in the surface layer (b), for particles with an initial diameter of 154 nm and 247 nm, respectively. The results are from a simulation with three different bulk phase oligomerization mechanisms: peroxyhemiacetal (R1a), hemiacetal (R3) and ester formation (R4) (k_f = 1.2x10^{-27} cm^3 molecules^{-1} and k_d = 1/3.2 h^{-1}), and surface layer oligomer formation by the reactive uptake of adsorbed pinonaldehyde (R1b, R2b and Eq. 33) (k_f = 3x10^{-15} cm^3 molecules^{-1} k_d = 3/2 h^{-1}).

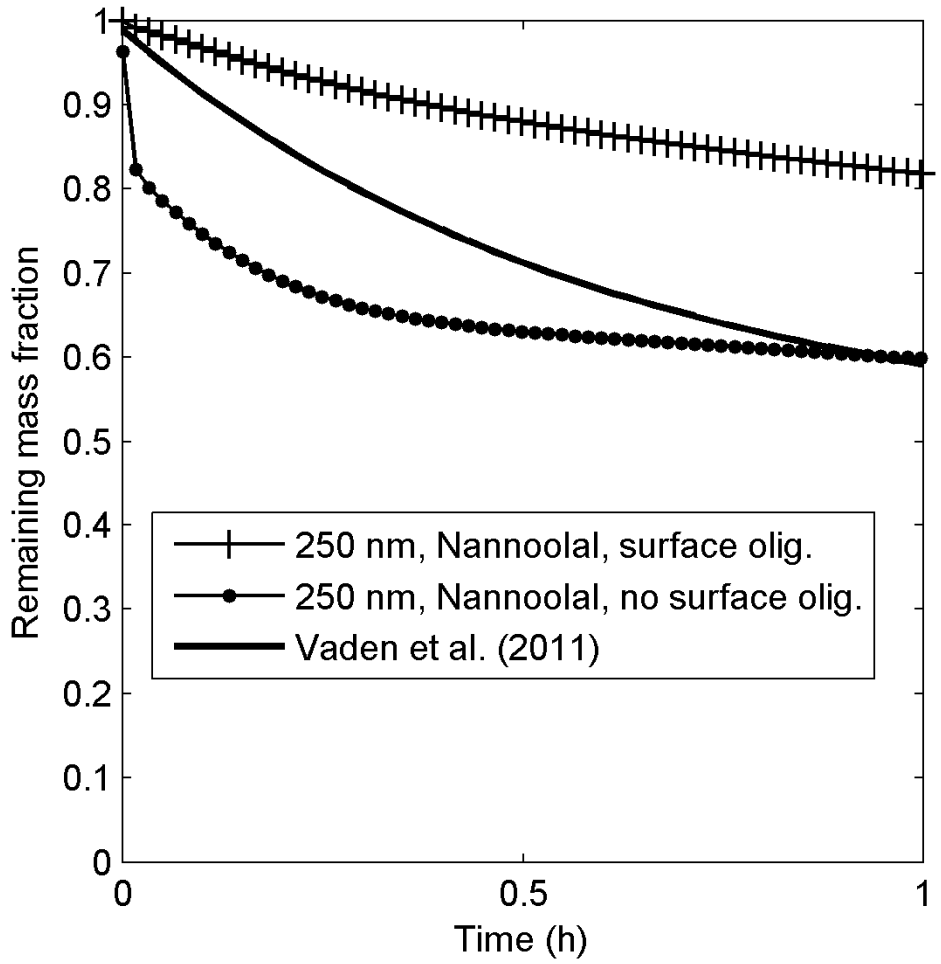

Figure S8. Modelled and measured (Vaden et al., 2011) remaining mass fractions during α-pinene SOA particle evaporation. The model results are from simulations with the vapour pressure method from Nannoolal et al. (2008) and with or without oligomer formation in the surface layer by the reactive uptake of adsorbed pinonaldehyde (R1b, R2b and Eq. 33) (k_f = 3x10^{-15} cm^3 molecules^{-1} k_d = 3/2 h^{-1}).

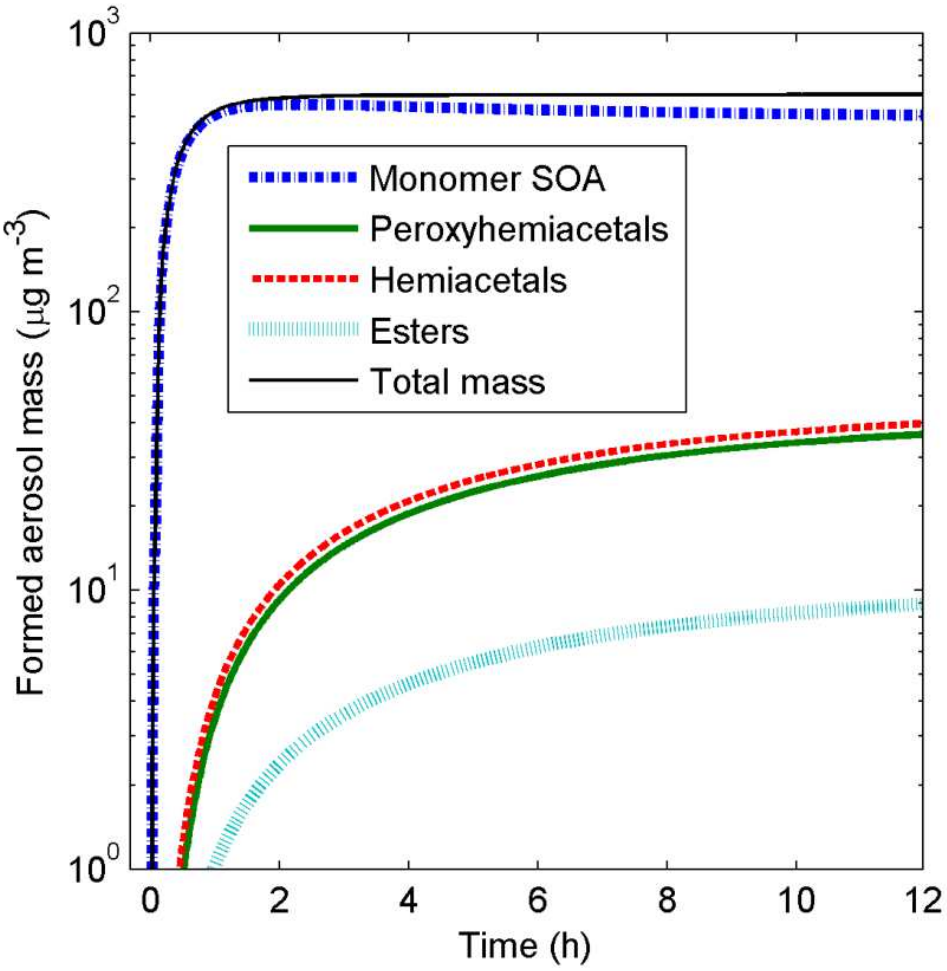

Figure S9. Modelled SOA composition when considering three different particle bulk phase oligomerization mechanisms: peroxyhemiacetal formation (R1a), hemiacetal formation (R3) and ester formation (R4) (k_f = 1.2x10^{-27} cm^3 molecules^{-1} and k_d = 1/3.2 h^{-1}).

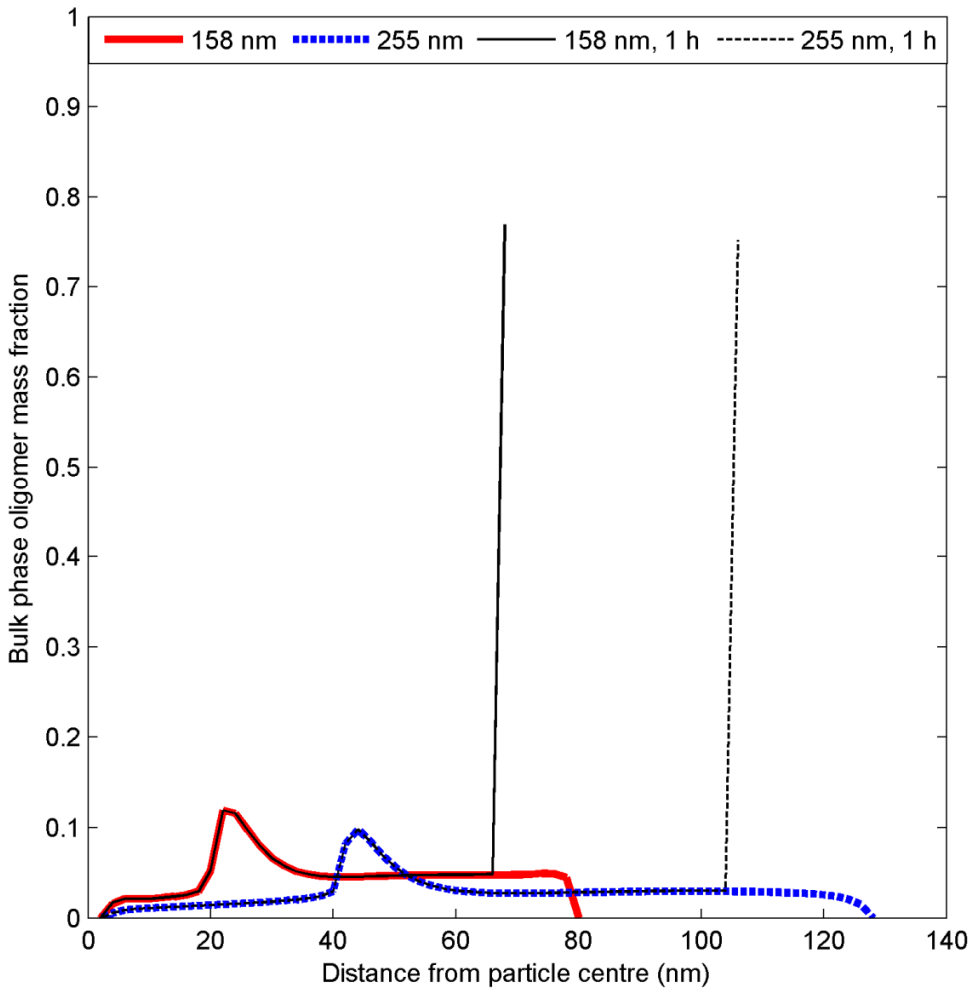

Figure S10. Modelled bulk phase oligomer mass fractions in the different particle layers at different distances from the particle centre at the start and after 1 hour of evaporation. The results are given for two particle sizes (D_p=158 and 255 nm, respectively). The oligomer SOA was assumed to be formed by a reaction between two of the least volatile MCMv.3.2 α-pinene oxidation products (C922OOH and C921OOH) ($k_f = 10^{-23}$ cm^3 molecules^{-1} and k_d = 1/22 h^{-1}).

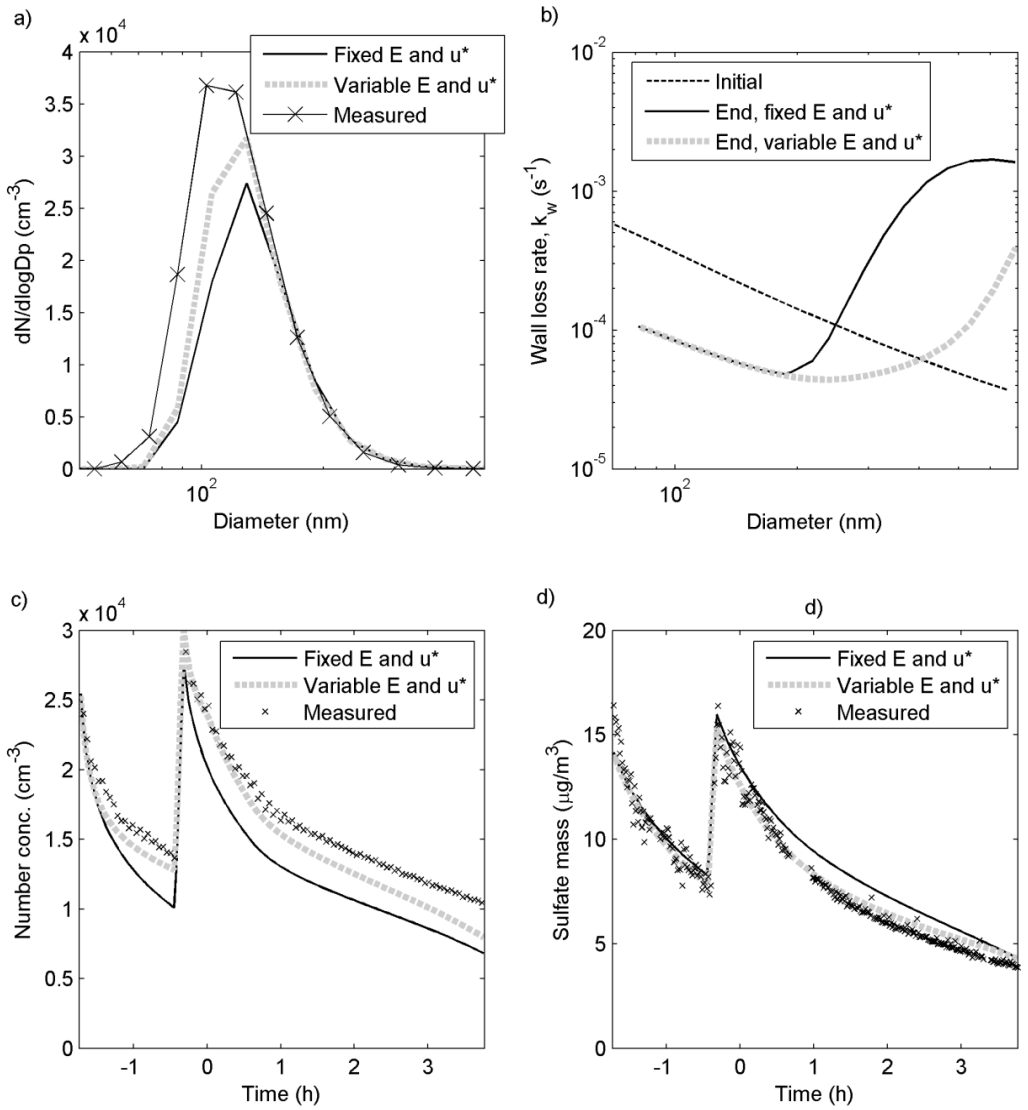

Figure S11. Modelled and measured a) particle number size distribution at the end of the *m*-xylene experiment, b) initial and final effective wall deposition loss rates (modelled), c) number concentration and d) sulphate seed aerosol mass concentration. The model results are from a simulation with a fixed $\overline{E}_t$ of 50 V cm^{-1} and a u^* of 0.05 m s^{-1} or variable $\overline{E}_t$ calculated with Eq. (34) and u^* = 0.01 m s^{-1} before the UV-lights are turned on and u^* = 0.05 m s^{-1} after the UV-lights are turned on.

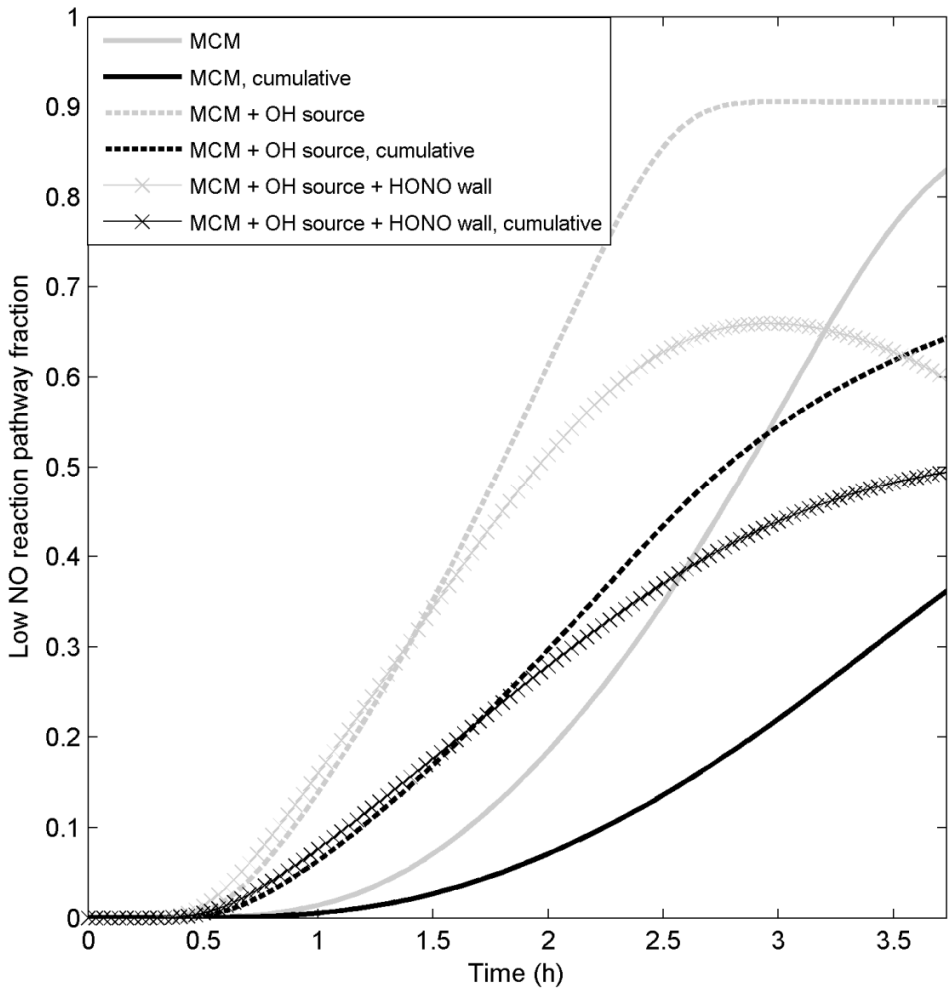

Figure S12. Modelled current time step and cumulative fraction of the *m*-xylene first generation RO_2 products that react (have reacted) with HO_2 instead of NO. The results are given for simulations with the original MCMv3.2 gas phase chemistry, with MCMv3.2 gas phase chemistry and an artificial OH source of 10^8 cm^3 s^{-1}, and with MCMv3.2 gas phase chemistry, the artificial OH source and wall emissions of HONO.

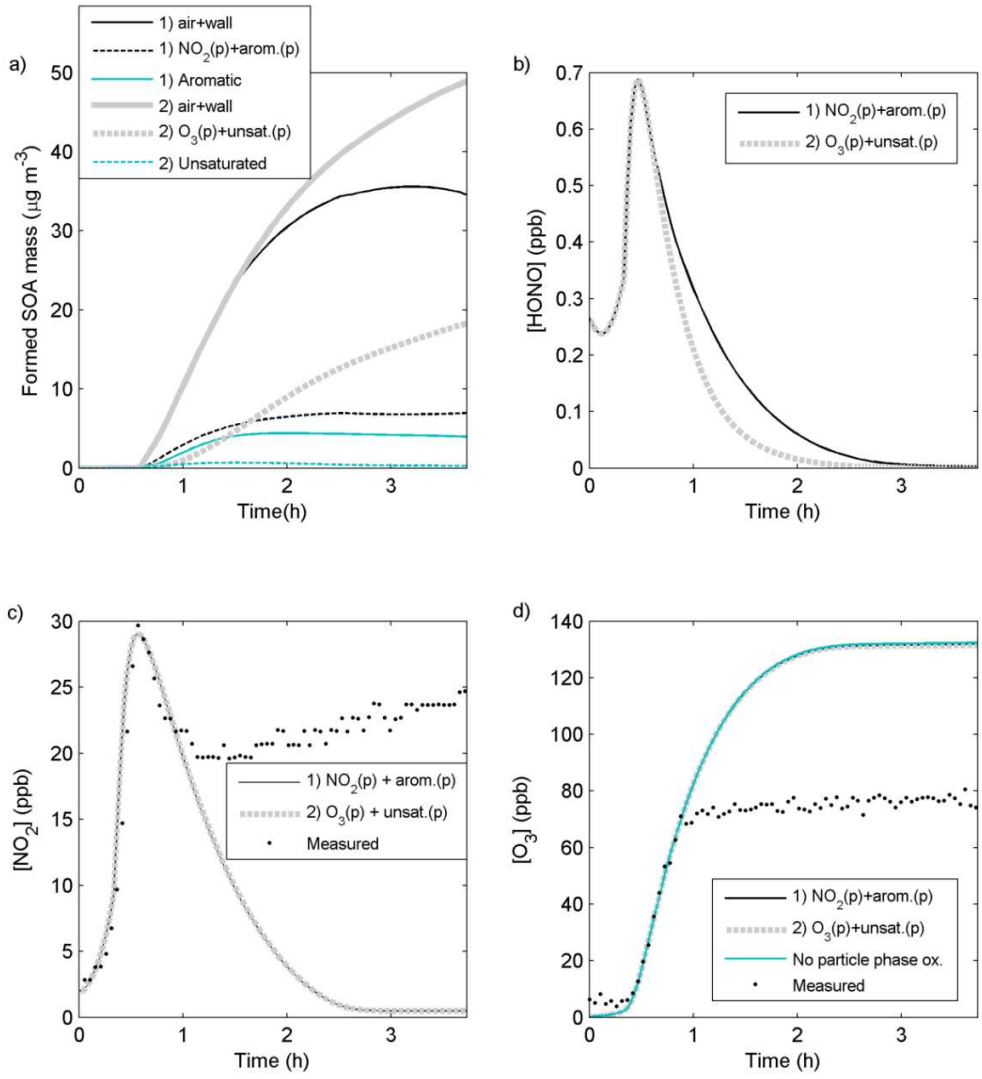

Figure S13. Results from simulations of the *m*-xylene oxidation experiment by Nordin et al. (2013) when considering 1) HONO formation from heterogeneous reactions (k_{NO_2} =10^{-15} cm^{-3} s^{-1} and D_{0,NO_2} =10^{-7} cm^2 s^{-1}) or 2) heterogeneous reactions of O_3 (k_{O_3} =10^{-16} cm^{-3} s^{-1} and D_{0,O_3} =10^{-7} cm^2 s^{-1}). For simulation Nr. 1 Fig. a shows the total SOA mass (air + wall), SOA mass of formed oxidation products from the reaction between the aromatic compounds and NO_2, and the remaining non reacted aromatic SOA mass. For simulation Nr. 2 Fig. a shows the total SOA mass, SOA mass of formed oxidation products from the heterogeneous O_3 reactions, and the remaining non reacted unsaturated organic SOA mass. Figure b shows the modelled HONO concentration, c) the NO_2 concentration and d) the O_3 concentration. In Fig. d we also included the results from a simulation without heterogeneous oxidation reactions.

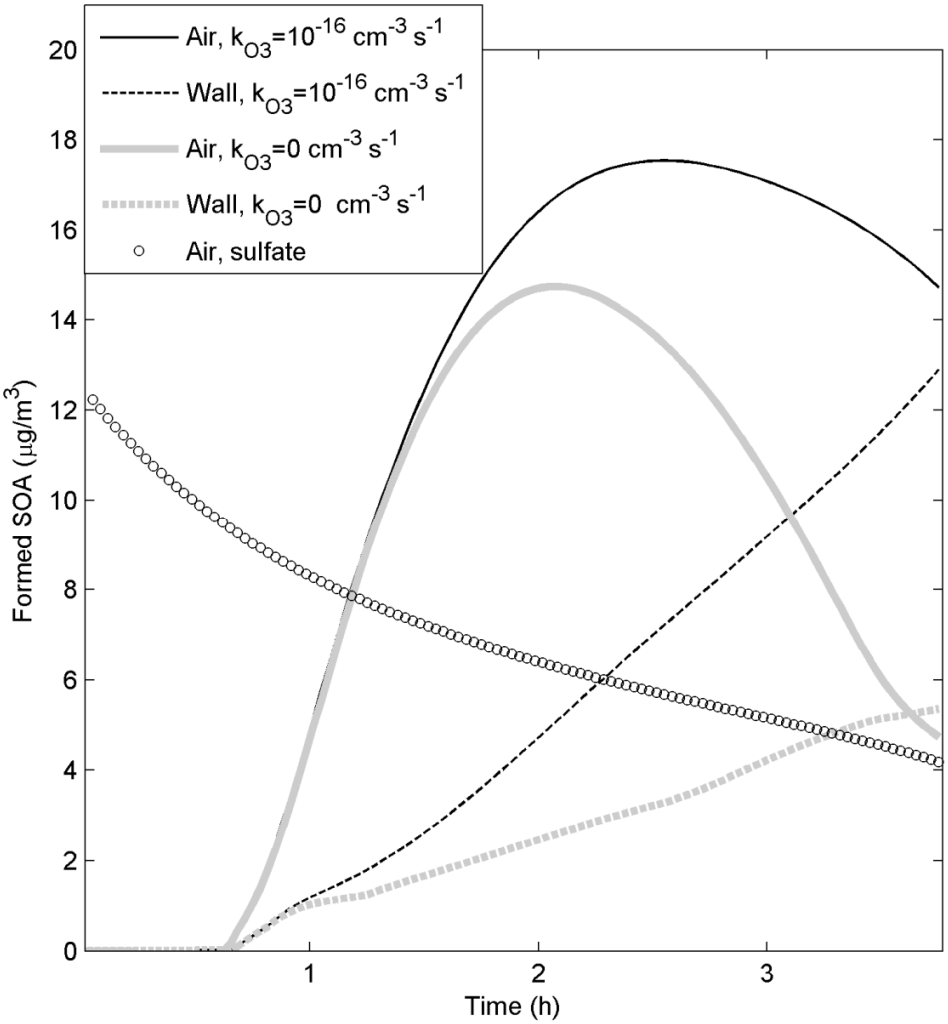

Figure S14. Modelled SOA mass formation in the air and on the wall deposited particles during the *m*-xylene oxidation experiment by Nordin et al. (2013). The results are from simulations with a laminar layer width (Δx) of 1.0 cm adjacent to the chamber walls and a first order loss rate from the near wall gas phase to the walls ($k_{g,w}$) of 1/6 s^{-1}. ADCHAM was either run without or with heterogeneous reactions between O_3 and the unsaturated organic compounds ($k_{O_3}=10^{-16}$ cm^{-3} s^{-1} and $D_{0,O_3}=10^{-8}$ cm^2 s^{-1}).

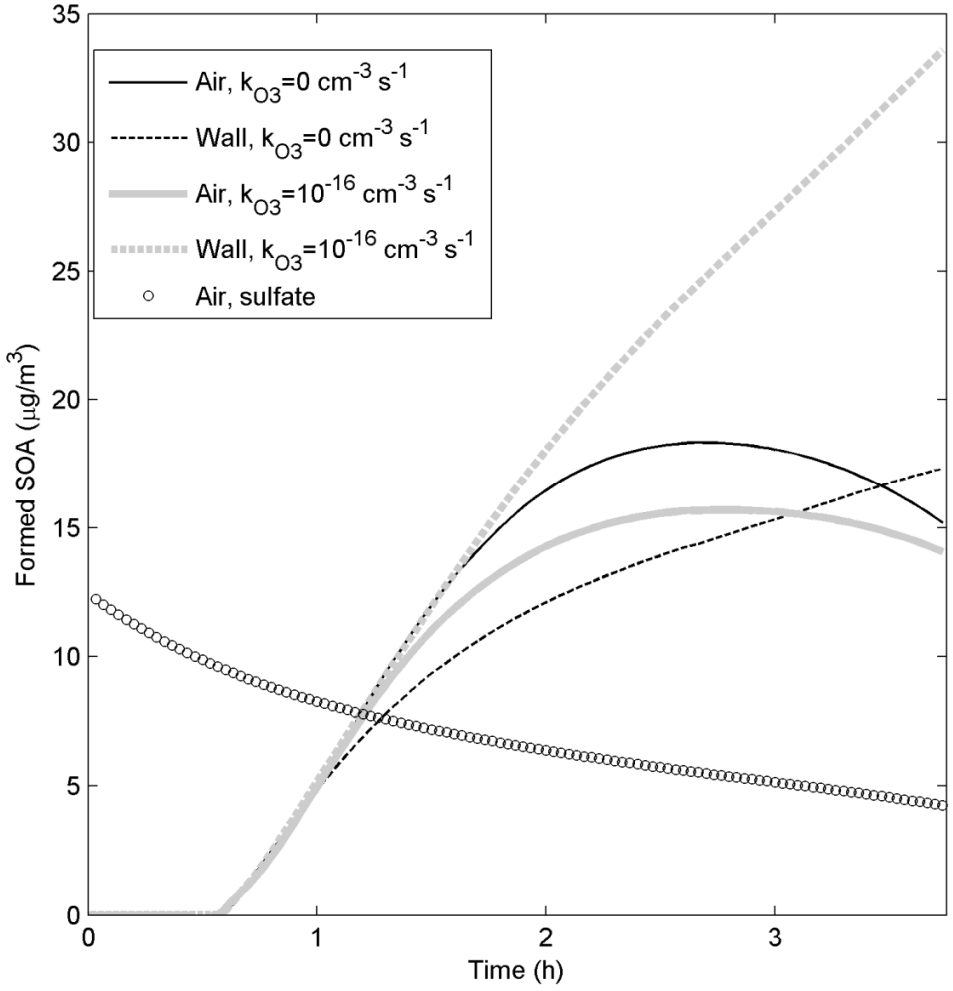

Figure S15. Modelled SOA mass formation in the air and on the wall deposited particles during the *m*-xylene oxidation experiment by Nordin et al. (2013). The results are from simulations with a laminar layer width (Δx) of 0.1 cm adjacent to the chamber walls and a first order loss rate from the near wall gas phase to the walls ($k_{g,w}$) of 1/20 s^{-1}. ADCHAM was either run without or with heterogeneous reactions between O_3 and the unsaturated organic compounds (k_{O_3} =10^{-16} cm^{-3} s^{-1} and D_{0,O_3} =10^{-8} cm^2 s^{-1}).

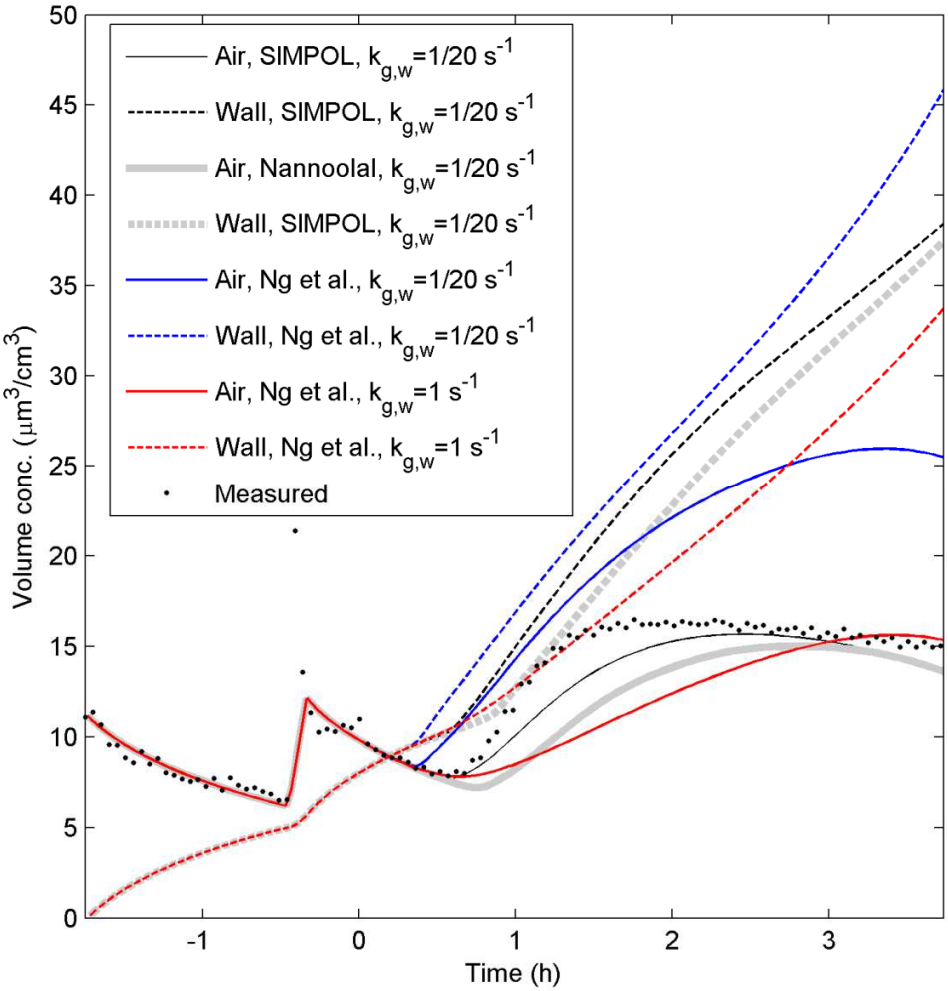

Figure S16. Modelled and measured volume concentrations (seed aerosol + SOA coating) during the *m*-xylene oxidation experiment by Nordin et al. (2013). The model results are from siumations with the SIMPOL (Pankow and Asher, 2008), Nannoolal et al. (2008) vapour pressure method or the semi-empirical parameterizations from Ng et al. (2007). The figure shows both the modelled particle volume concentrations in the air and on the walls.

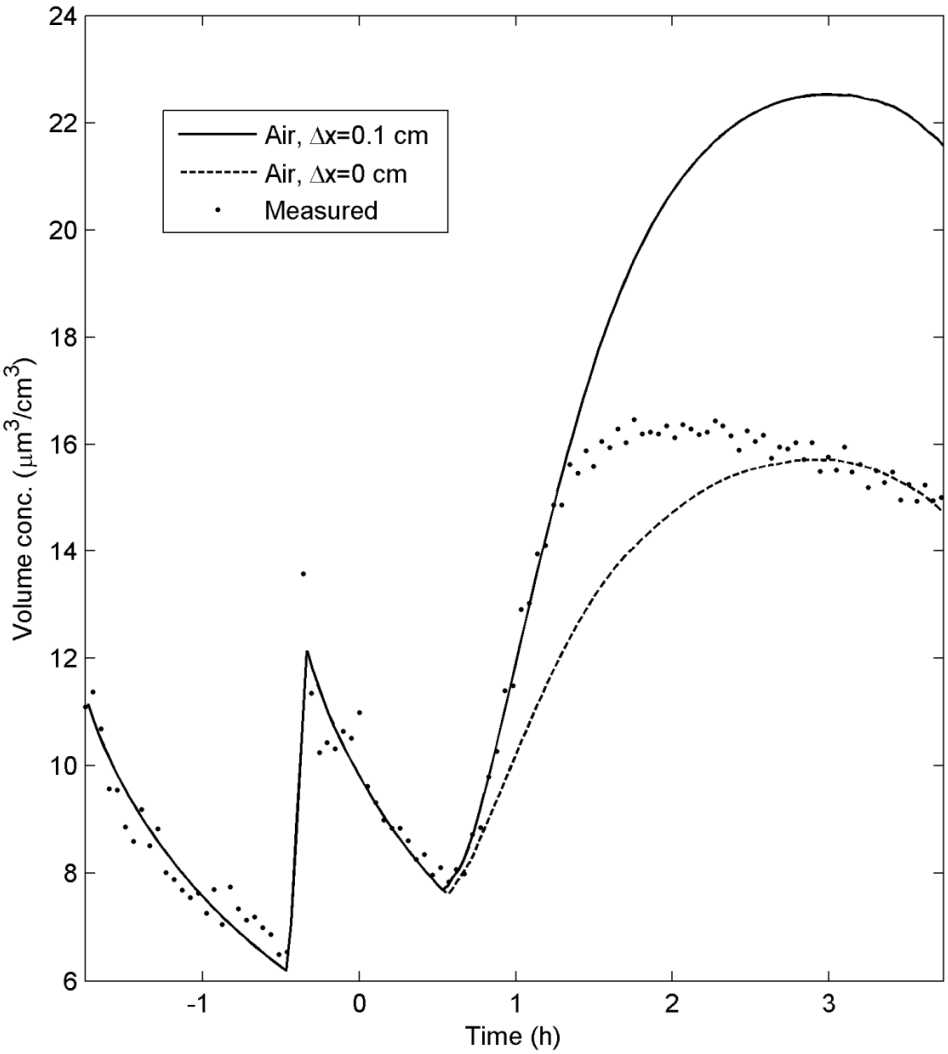

Figure S17. Modelled and measured particle volume concentrations in the air from the *m*-xylene oxidation experiment by Nordin et al. (2013). The model results are from simulations with a laminar layer of 0 or 0.1 cm adjacent to the chamber walls and without uptake of organic compounds directly onto the Teflon walls.